Vitalii Yaropud [1], Elchyn Aliiev [2], Ihor Mazur [1], Serhii Burlaka [1]

Vinnytsia National Agrarian University (1), Dnipro State Agrarian and Economic University (2)
ORCID: 1. 0000-0003-0502-1356, 2. 0000-0003-4006-8803; 3. 0000-0001-6619-810X; 4. 0000-0002-4079-4867

doi:10.15199/48.2023.09.11

Simulating the Process of Operation of Vortex Layer Electromagnetic Apparatus with Ferromagnetic Working Elements

***Abstract**. The article presents the results of the simulation of the work process of the electromagnetic apparatus of the vortex layer with ferromagnetic working elements on the example of the processing of liquid pig manure. As a result of analytical studies of the process of interaction of cylindrical ferromagnetic elements with a magnetic field in the working chamber of the vortex layer apparatus, the appropriate physical and mathematical apparatus was improved, which is the basis of numerical modeling in the STAR-CCM+ software package.*

Streszczenie. *W artykule przedstawiono wyniki symulacji procesu pracy aparatury elektromagnetycznej warstwy wirowej z ferromagnetycznymi elementami roboczymi na przykładzie procesu przetwarzania gnojowicy świńskiej. W wyniku badań analitycznych procesu oddziaływania cylindrycznych elementów ferromagnetycznych z polem magnetycznym w komorze roboczej aparatu warstwy wirowej ulepszono odpowiednią aparaturę fizyko-matematyczną, która jest podstawą modelowania numerycznego w programie STAR-CCM+ pakiet oprogramowania. (**Symulacja procesu działania aparatury elektromagnetycznej warstwy wirowej z ferromagnetycznymi elementami roboczym**i)*

Keywords: simulation, electromagnetic field, vortex layer apparatus, ferromagnet, processing, liquid manure.
Słowa kluczowe: symulacja, pole elektromagnetyczne, aparat warstwy wirowej, ferromagnes, obróbka, gnojowica.

Introduction

Vortex layer electromagnetic apparatuses with ferromagnetic working elements are intended for intensification of various physical and chemical processes. The apparatuses are hermetic, have no dynamic seals and consist of an electromagnetic device with cooling system, a process chamber and a control panel [1].

Physical and chemical processes in vortex layer electromagnetic apparatuses are intensified due to intensive mixing and dispersion of components being processed, acoustic and electromagnetic processing, high local pressure, etc. [2].

Numerous factors existing in the vortex layer and able to directly affect the raw materials being processed require the developers of devices and technological processes to know the essence of the phenomena and patterns taking place during processing of multicomponent systems [1–2].

Studies conducted in recent years [1-6] show that the apparatuses can be effectively used for: obtaining multicomponent suspensions and emulsions; extraction of protein substances from yeast cells; increasing the microbiological stability of food products and yeast activation in bakery production; improving the quality of semi-finished products and finished meat and fish products; intensification of extraction processes, particularly in cooking of broths, production of berry drinks and pectin; intensification of liquid manure and industrial wastewater treatment processes (disinfection, homogenization, mixing) in the course of their composting, etc.

It follows from analysis of literary sources [7-10] that vortex layer apparatuses are equipped with different types of working bodies and have various working area layouts. In the course of liquid-phase processes, using ferromagnetic elements as working bodies, trap screens or labyrinths designed to keep ferromagnetic particles in the working area may be installed on the ends of non-magnetic insert (or at the outlet only). Grinding and mixing may take place not only with the help of ferromagnetic particles, but also with the help of knives, tubes or rotors. In these cases, sieves act as filters (separators). Ferromagnetic elements are added to the working area using the electromagnetic dispenser.

Analyzing the results of previous research [1-10], one can state that efficiency of the vortex layer apparatus is proposed to be increased due to design improvement and justification of structural and technological parameters of individual systems, without regard to interconnection between them. It should also be noted that most of the results obtained from substantiation of structural and technological parameters are experimental in their nature, having no theoretical basis.

Investigation of the process of electromagnetic field change in the working chamber of the vortex layer apparatus

The first stage of theoretical research lies in determination of the basic parameters of rotating electromagnetic field in the working chamber of the apparatus, which is generated by the inductor coils being alternately switched on/off at respective time intervals: electromagnetic field intensity (H, A/m); magnetic flux density, magnetic induction (V, T) and electromagnetic field's vector potential (A, Tl·m).

Given that electromagnetic field rotates, we will determine functional dependences for H, B, and A in the working chamber of the vortex layer apparatus using STAR- CCM+ software package [11–15]. To do this, we will generate the 3D model of the vortex layer apparatus's main regions, where electromagnetic fields act and originate (fig. 1).

The multifaceted cell and surface grid generator was chosen as the grid model. The basic size of the cell was 0.01 m. General appearance of the resulting grid with geometric dimensions and selected areas is shown in fig. 2.

Separate physical models of the continuum, reference values and starting conditions were selected for each area (fig. 2).

For the inductor coil area, the following was chosen: a three-dimensional model of continuous medium with a non-stationary implicit pattern; an electromagnetism model with finite-volume magnetic vector potential and eddy current suppression [16] and excitation coil model. The coil material is copper with the following properties: magnetic permeability - $1.25663 \cdot 10^{-6}$ Hn /m; electrical conductivity – 5, $96 \cdot 10^7$ cm/m. For the coil core region, the following was chosen: a three-dimensional model of continuous medium with non-stationary implicit pattern; an electromagnetism model with finite-volume magnetic vector potential and eddy current suppression. The coil material is steel with the following properties: magnetic permeability – $1.25663 \cdot 10^{-6}$ Hn/m; electrical conductivity – $3.78 \cdot 10^7$ cm/m.

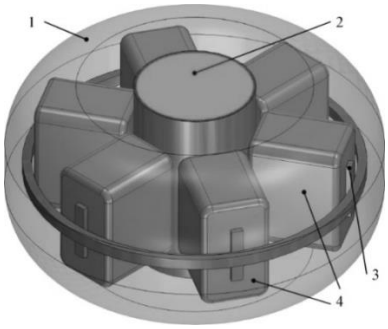

Fig. 1. 3D model of the main areas and elements of the vortex layer apparatus: 1 – inductor housing with transformer oil; 2 – working chamber; 3 – coil core; 4 – inductor coils

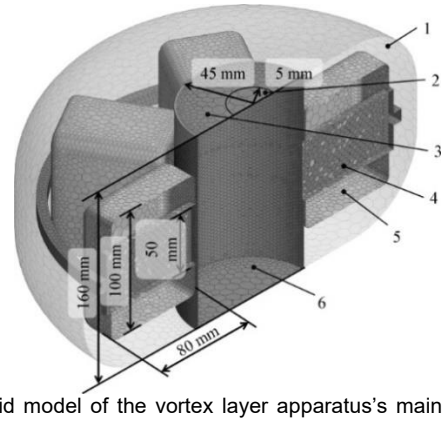

Fig. 2. Grid model of the vortex layer apparatus's main areas and elements: 1 – inductor housing area; 2 – additional component supply hole; 3 –mixture supply hole; 4 – coil core region; 5 –inductor coil area; 6 –working chamber area

For the inductor body area, the following was chosen: a three-dimensional model of continuous liquid of constant density with non-stationary implicit pattern; fluid movement is separate and turbulent, which is subject to k-ε turbulence model and Reynolds averaging of Navier-Stokes equation; an electromagnetism model with finite-volume magnetic vector potential and eddy current suppression. The region's environment is transformer oil with the following properties: density – 895 kg/m$^{3;}$ dynamic viscosity – 198.2 Pa·s; magnetic permeability – $1.25663 \cdot 10^{-6}$ Hn/m and electrical conductivity – $1.0 \cdot 10^{-10}$ S/m.

For the working chamber area, the following was chosen: a three-dimensional model of continuous multiphase medium of constant density with non-stationary implicit pattern; the medium's movement is separate and turbulent, which is subject to k-ε turbulence model and Reynolds averaging of Navier-Stokes equation; an electromagnetism model with finite-volume magnetic vector potential and eddy current suppression. The region's environment is liquid manure with the following properties: density – 997.561 kg/m$^{3;}$ dynamic viscosity – $8.8871 \cdot 10^{-4}$ Pa·s; magnetic permeability – $1.25663 \cdot 10^{-6}$ Hn/m; electrical conductivity – $5.5 \cdot 10^{-6}$ cm/m.

The factors of numerical modeling were chosen as follows: the coil's maximum magnetomotive force ξ_{max} (6000–36000 A•turns; electromagnetic field's rotation frequency n (1000–5000 rpm).

Let us plot the electromagnetic field rotation in STAR-CCM+ software package by changing each coil's magnetomotive force value (numbering the coils clockwise from 1 to 6) to 0 or ξ_{max} according to the algorithm

$$(1) \quad if\ \left(sin\left[\frac{n \cdot t \cdot \pi}{60} - \frac{(N-1)\pi}{3}\right] < sin\frac{4\pi}{3}\right)\{\xi_N = -\xi_{max}\}$$

$$else\left\{if\ \left(sin\left[\frac{n \cdot t \cdot \pi}{60} - \frac{(N-1)\pi}{3}\right] > sin\frac{\pi}{3}\right)\{\xi_N = \xi_{max}\}\ else\ \{\xi_N = 0\}\right\}$$

where if ( ) { } else { } is "if" operator; n is the electromagnetic field rotation frequency, rpm; ξ_{max} is the coil's maximum magnetomotive force, A•turns; t – time, s; N is the clockwise coil number.

When simulating, we assume that the change in the coil's magnetomotive force occurs instantaneously. This causes the electromagnetic field's instantaneous rotation by the angle of 60°.

As a result of numerical modeling, the visualization of electromagnetic field intensity vector H, magnetic induction B and electromagnetic field vector potential d A in the vortex layer apparatus was obtained for the accepted value of the magnetomotive force of only two opposite coils ξ_{max} = 5000 A•turns, which is shown in fig. 3.

For further calculations, distribution of electromagnetic indicators in the working chamber of the vortex layer apparatus is presented in the form of respective tensors stored in the form of a text file with a set of numerical values. The regression equation of electromagnetic parameters in the working chamber of the vortex layer apparatus depending on the coordinates cannot be constructed due to the relationship's complex nature. Therefore, respective regularities are presented in the form of graphs for each plane of the space section: XOY, XOZ, YOZ in fig. 4.

To evaluate the impact of research factors (the coil's maximum magnetomotive force ξ_{max}, A•turns; electromagnetic field rotation frequency n, rpm) we obtain the regularity of change in minimum and maximum values of electromagnetic indicators in the working chamber of the vortex layer apparatus.

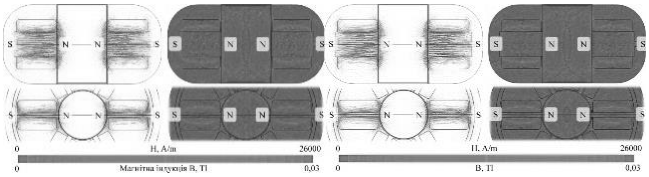

Fig. 3. Distribution of electromagnetic indicators in the vortex layer apparatus for accepted value of the magnetomotive force of only two opposite coils ξ_{max} = 5000 A·turns

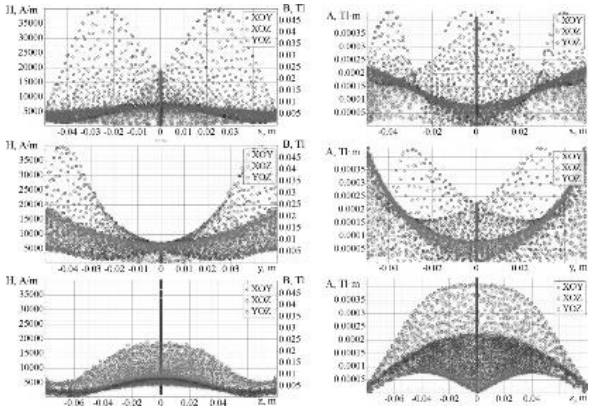

Fig. 4. Dependencies between electromagnetic indicators in the working chamber of the vortex layer apparatus and coordinates for accepted value of the magnetomotive force of only two opposite coils ξ_{max} = 5000 A·turns

Hence, we obtained the following dependencies of:
– electromagnetic field strengths:

$$(2) \quad H_{max} = 88.5855 - 0.0688326\ n + 0.00001231\ n^2 + 89.0451\ \xi_{max} - 0.001832\ n\ \xi_{max} - 0.003642\ \xi_{max}^2,$$

$$H_{min} = -3393.23 + 2.38901\,n - 0.000397502\,n^2 + 14.6202\,\xi_{max} - 0.0005823\,n\,\xi_{max} - 0.00153\,\xi_{max}^2,$$

– magnetic induction:

$$B_{max} = 0{,}0013268 - 9{,}517\cdot10^{-7}\,n + 1{,}666\cdot10^{-10}\,n^2 + 0{,}000708\,\xi_{max} - 8{,}39\cdot10^{-9}\,n\,\xi_{max} - 5{,}39\cdot10^{-9}\,\xi_{max}^2, \quad (3)$$

$$B_{min} = -0{,}028426 + 0{,}00002\,n - 3{,}33008\cdot10^{-9}\,n^2 + 0{,}00012\,\xi_{max} - 4{,}878\cdot10^{-9}\,n\,\xi_{max} - 1{,}28\cdot10^{-8}\,\xi_{max}^2,$$

– electromagnetic field vector potential:

$$A_{max} = -0.0000239 + 1.668\cdot10^{-8}\,n - 2.7\cdot10^{-12}\,n^2 + 6.5\cdot10^{-6}\,\xi_{max} - 1.98\cdot10^{-11}\,n\,\xi_{max} - 4.08\cdot10^{-11}\,\xi_{max}^2, \quad (3)$$

$$A_{min} = 0.0001459 - 1.0359\cdot10^{-7}\,n + 1.727\cdot10^{-11}\,n^2 + 1.9\cdot10^{-6}\,\xi_{max} - 3.83\cdot10^{-10}\,n\,\xi_{max} - 2.53\cdot10^{-10}\,\xi_{max}^2.$$

The dependencies presented above are used in further analytical studies of interaction between ferromagnetic elements and rotating magnetic field, and in subsequent numerical modeling of the process of mixture components grinding and their mixing in the working chamber of the vortex layer apparatus.

Study of the process of interaction between ferromagnetic elements and magnetic field in the working chamber of the vortex layer apparatus

The second stage involves theoretical studies of the process of interaction between cylindrical ferromagnetic elements and magnetic field in the working chamber of the vortex layer apparatus (fig. 5).

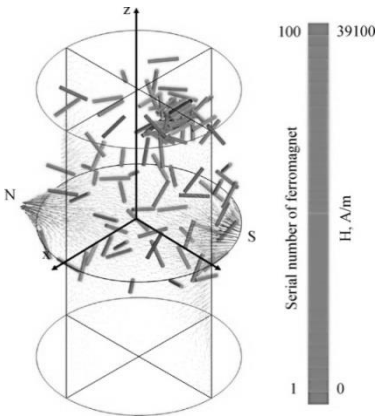

Fig. 5. Visualization of the interaction between ferromagnetic elements and magnetic field in the working chamber of the vortex layer apparatus in STAR-CCM+ software package

In the chamber of the vortex layer apparatus, cylindrical ferromagnetic elements are magnetized to saturation. Therefore, they can be considered as magnetic dipoles, located in rotating electromagnetic field. Further analytical models will be based on research by Oberemok V.M., Nikytenko M.I. [2], Logvinenko D.D., Shelyakov O.P. [1], Ibragimov R.A. and others. [17–18]. Thus, according to [19], a couple of forces act on ferromagnetic elements in rotating external electromagnetic field, these forces trying to turn it in the direction of the field vector:

$$M_n = MH\sin\varphi, \quad (5)$$

where φ is the angle between the ferromagnetic element's magnetic moment vector (coinciding with the largest axis) and magnetic field intensity vector $\overline{H}$; M is the magnetic moment of the ferromagnetic element under conditions of its full saturation:

$$M = I_M \cdot \Omega, \quad (6)$$

where I_m is the magnetic moment per unit volume of ferromagnetic element; Ω is the volume of the cylindrical ferromagnetic element, m^3:

$$\Omega = \frac{\pi}{4} D_\Omega^2 L_\Omega, \quad (7)$$

where D_Ω is the diameter of the base of the ferromagnetic element, m; L_Ω is the length of the ferromagnetic element, m.

Under the torque action, the cylindrical ferromagnetic element rotates with angular velocity ω_{abs}, which equals to the sum of relative ω_{rel} and transfer ω velocities:

$$\omega_{abs} = \omega_{rel} + \omega. \quad (8)$$

Transfer velocity equals to electromagnetic field rotation velocity

$$\omega = 2\pi\frac{n}{60}. \quad (9)$$

Let us determine the ferromagnetic element's relative velocity. To do this, we write down respective differential equation of the ferromagnetic element's motion in relation to the stationary vector of electromagnetic field intensity $\overline{H}$:

$$I_\Omega\ddot{\varphi} = MH\sin\varphi, \quad (10)$$

where I_Ω is the inertia moment of the cylindrical ferromagnetic element:

$$I_\Omega = \frac{m_\Omega L_\Omega^2}{12} = \frac{\pi}{4} D_\Omega^2 L_\Omega \rho_\Omega \frac{L_\Omega^2}{12} = \frac{\pi}{48}\rho_\Omega D_\Omega^2 L_\Omega^3. \quad (11)$$

Considering (6), (7) and (11), equation (10) takes the following form

$$\ddot{\varphi} = \frac{12 I_M H}{\rho_\Omega L_\Omega^2}\sin\varphi. \quad (12)$$

Starting conditions of equation (12):

$$\begin{cases}\varphi|_{t=0} = \varphi_0,\\ \dot{\varphi}|_{t=0} = 0.\end{cases} \quad (13)$$

Differential equation (12) together with (13) was solved by Lyapunov's approximate method through Jacobi function in [1–2]:

$$\dot{\varphi} = -\left(\varphi_0 + \frac{1}{192}\varphi_0^2\right)\frac{\frac{12 I_M H}{\rho_\Omega L_\Omega^2}}{1+\frac{\varphi_0^2}{16}}\sin\left(\frac{\frac{12 I_M H}{\rho_\Omega L_\Omega^2}}{1+\frac{\varphi_0^2}{16}}t\right) + \frac{1}{192}\varphi_0^3\frac{\frac{12 I_M H}{\rho_\Omega L_\Omega^2}}{1+\frac{\varphi_0^2}{16}}\sin\left(3\frac{\frac{12 I_M H}{\rho_\Omega L_\Omega^2}}{1+\frac{\varphi_0^2}{16}}t\right). \quad (14)$$

Using the demagnetization factor expression in [1–2], the relative speed of a ferromagnetic element is:

$$\dot{\varphi} = \omega_{rel} = -\left(\varphi_0 + \frac{1}{192}\varphi_0^3\right)\frac{3{,}464HX}{L_\Omega Y}\times \times\sin\left(\frac{3{,}646HX}{L_\Omega Y}t\right) + \frac{1}{192}\varphi_0^3\frac{10{,}39HX}{L_\Omega Y}\sin\left(\frac{10{,}39HX}{L_\Omega Y}t\right),$$

$$X = \sqrt{\frac{\mu-1}{\left[1+(\mu-1)\frac{\frac{\lambda}{\sqrt{\lambda^2-1}}\ln\left(\lambda+\sqrt{\lambda^2-1}-1\right)}{\lambda^2-1}\right]\rho_\Omega}}, \quad (15)$$

$$Y = 1+\frac{\varphi_0^2}{16},\ \lambda = \frac{L_\Omega}{D_\Omega},$$

where μ is magnetic permeability.

In the working chamber of the vortex layer apparatus, the following forces act on each cylindrical ferromagnet.

1. Displacement force of the cylindrical ferromagnet under the action of rotating electromagnetic field [2]:

$$\overline{F_M} = \chi\Omega\overline{H}\left(\overline{\nabla}\cdot\overline{H}\right) = \chi\frac{\pi}{4}D_\Omega^2 L_\Omega\overline{H}\left(\overline{\nabla}\cdot\overline{H}\right) \quad (16)$$

where X is the magnetic susceptibility of the cylindrical ferromagnet material.

2. Gravity forces [20]:

$$\overline{F_g} = \frac{\pi}{4}D_\Omega^2 L_\Omega\rho_\Omega\overline{g}, \quad (17)$$

where $\overline{g}$ is the free fall acceleration, m/s^2.

3. Archimedes' force:

$$\overline{F_A} = \frac{\pi}{4} D_\Omega^2 L_\Omega \rho_l \overline{g}, \tag{18}$$

where ρ_l is the liquid density, kg/m^3.

4. The force caused by the pressure change in the flow direction due to its acceleration [21]:

$$\overline{F_{ac}} = \frac{\pi}{4} D_\Omega^2 L_\Omega \rho_l \frac{d_l \overline{V_l}}{dt}, \quad \frac{d_l}{dt} = \frac{\partial}{\partial t} + \overline{V_l} \cdot \overline{\nabla}, \tag{19}$$

where $\overline{V_l}$ is liquid velocity vector, m/s.

5. The viscous resistance force that occurs when the cylindrical ferromagnet moves with particular relative velocity in the fluid flow:

$$\overline{F_D} = = \frac{1}{8}\left(\frac{\pi}{2} D_\Omega^2 + 2\pi D_\Omega L_\Omega\right) \rho_l f_M(Re)\left(\overline{V_l} - \overline{V_\Omega}\right)\left|\overline{V_l} - \overline{V_\Omega}\right|, \tag{20}$$

where $f_M(Re)$is the viscous resistance factor.

6. The total force of ferromagnets' contact interaction between themselves and the working chamber wall, which is based on Hertz-Mindlin spring-damper contact model [22]:

$$\bar{F}_{cont} = = \begin{cases} \left(-K_n \overline{d_n} - N_n \overline{V_n}\right) + \left(-K_t \overline{d_t} - N_t \overline{V_t}\right), & \overline{S_{pA}} = \overline{S_{pB}}, \\ 0, & \overline{S_{pA}} \neq \overline{S_{pB}}; \end{cases} \tag{21}$$

where $K_n = 4E_{eq}\sqrt{d_n R_{eq}}/3$is the elastic component's normal stiffness factor, kg/s^2; $N_n = \sqrt{(5K_n M_{eq})} N_{n\ damp}$– the damping component's normal damping ratio, kg/s; $K_t = 8G_{eq}\sqrt{d_t R_{eq}}$– elastic component's tangential stiffness ratio, kg/s^2; $N_t = \sqrt{(5K_t M_{eq})} N_{t\ damp}$ – the damping component's tangential damping ratio, kg/s; $\overline{V_n}$ and $\overline{V_t}$ are normal and tangential components of the ferromagnet surface's relative velocity at the point of contact, m/s; $N_{damp}$is the attenuation coefficient; $R_{eq} = (2/D_A + 2/D_B)^{-1}$ is the equivalent radius of two ferromagnets A and B, m; $E_{eq} = \left((1-\nu_A^2)/E_A + (1-\nu_B^2)/E_B\right)^{-1}$ is the equivalent Young's modulus of two ferromagnets A and B, Pa; $M_{eq} = \left(M_A^{-1} + M_B^{-1}\right)^{-1}$ is the equivalent mass of two ferromagnets A and B, kg; $G_{eq} = (2(2-\nu_A)(1+\nu_A)/E_A + 2(2-\nu_B)(1+\nu_B)/E_B)^{-1}$ is the equivalent shear modulus of two ferromagnets A and B, Pa; d_n, d_t is a virtual overlap of ferromagnets A and B in normal and tangential directions, m; M_A, M_B are the masses of seeds A and B (for surface $M_{wall} = \infty$), kg; D_A and D_B are effective diameters of ferromagnets A and B (for surface $D_{wall} = \infty$), m; E_A and E_B are Young's moduli of ferromagnets A and B, Pa; ν_A and ν_B are Poisson ratios of ferromagnets A and B.

Based on the formulas presented above, we obtain the equations of cylindrical ferromagnets movement in a fluid flow under the action of rotating electromagnetic field:

$$\begin{cases} \frac{\pi}{4} D_\Omega^2 L_\Omega \rho_\Omega \frac{d_\Omega \overline{V_\Omega}}{dt} = \overline{F_M} + \overline{F_g} + \overline{F_A} + \overline{F_{ac}} + \overline{F_D} + \overline{F_{cont}}, \\ \frac{d_\Omega \overline{S_\Omega}}{dt} = \overline{V_\Omega}, \quad \frac{d_\Omega}{dt} = \frac{\partial}{\partial t} + \overline{V_\Omega} \cdot \overline{\nabla}. \end{cases} \tag{22}$$

Substituting (16)–(21) into (225), we finally obtain:

Joint solution of differential equations' systems (15) and (23) in general is impossible by analytical methods. Investigations [23] proposed the solution of similar systems using the finite element method, which is implemented in STAR-CCM+.

$$\begin{cases} \frac{d_\Omega \overline{V_\Omega}}{dt} = \frac{\chi}{\rho_\Omega} \overline{H}\left(\overline{\nabla} \cdot \overline{H}\right) + \overline{g} + \frac{\rho_l}{\rho_\Omega}\overline{g} + \frac{\rho_l}{\rho_\Omega}\frac{d_l \overline{V_l}}{dt} + \\ + \left(\frac{1}{4L_\Omega} + \frac{1}{D_\Omega}\right)\frac{\rho_l}{\rho_\Omega} f_M\left((Re)\left(\overline{V_l} - \overline{V_\Omega}\right)\left|\overline{V_l} - \overline{V_\Omega}\right| \frac{4}{\pi \rho_\Omega D_\Omega^2 L_\Omega} \bar{F}_{cont}, \right) \\ \frac{d_\Omega \overline{S_\Omega}}{dt} = \overline{V_\Omega}, \quad \frac{d_\Omega}{dt} = \frac{\partial}{\partial t} + \overline{V_\Omega} \cdot \overline{\nabla}, \quad \frac{d_l}{dt} = \frac{\partial}{\partial t} + \overline{V_l} \cdot \overline{\nabla}, \\ \bar{F}_{cont} = \begin{cases} \left(-K_n \overline{d_n} - N_n \overline{V_n}\right) + \left(-K_t \overline{d_t} - N_t \overline{V_t}\right), \overline{S_{pA}} = \overline{S_{pB}}, \\ 0, \quad \overline{S_{pA}} \neq \overline{S_{pB}}; \end{cases} \end{cases} \tag{23}$$

The following physical models are adopted for simulation of ferromagnets in STAR-CCM+: Lagrangian multiphase, discrete element method, existence time, two-way communication, constant density, resistance force and mixed particles. Multiphase interaction between ferromagnets and the wall obeyed Hertz-Mindlin model.

Ferromagnets' parameters are as follows: Poisson's ratio – 0.3; Young's modulus – $2.0 \cdot 10^{11}$ Pa; density – 7800 kg/m^3; base diameter – 2 mm. For ferromagnet-ferromagnet interaction: rest friction ratio – 0.6; normal recovery factor – 0.5; tangent recovery ratio – 0.5; rolling resistance ratio being 0.001. For ferromagnet- wall interaction: rest friction ratio – 0.7; normal recovery factor – 0.5; tangent recovery ratio – 0.5; rolling resistance ratio being 0.001.

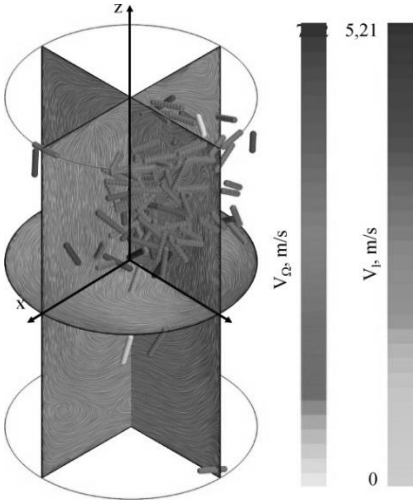

Fig. 6. Visualization of ferromagnets V_Ω and liquid V_l velocity distribution in the working chamber of the vortex layer apparatus under the action of rotating electromagnetic field in STAR-CCM+

The simulation was carried out using a non-stationary implicit pattern with a step of 0.001s per 60 s. Visualization of the result of ferromagnets' movement simulation under the action of rotating electromagnetic field is shown in fig. 5–7. Fig. 5 shows the distribution of ferromagnets V4 $_\Omega$ and liquid V_l velocities in the working chamber of the vortex layer apparatus. Fig. 6–7 correspond to visualization of distribution of the contact interaction force of F_{cont} ferromagnets and the frequency of ferromagnets' impacts ' per time unit κ.

Maximum strength of electromagnetic field H (2000–10000 A/m), frequency of electromagnetic field rotation n (1000–3000 rpm), number of ferromagnets N (100–500 pieces), ferromagnet length L_M (0.02–0.04 m).

The criteria for process evaluation were chosen as follows: the average speed of ferromagnet movement V_Ω in the working chamber of the vortex layer apparatus, the maximum force of ferromagnets' contact interaction F_{cont}, the frequency of ferromagnets' impacts per time unit κ.

As a result of numerical simulation in STAR-CCM+ according to the comprehensive research plan (3^4 = 81 numerical experiment), the values of specified criteria were obtained.

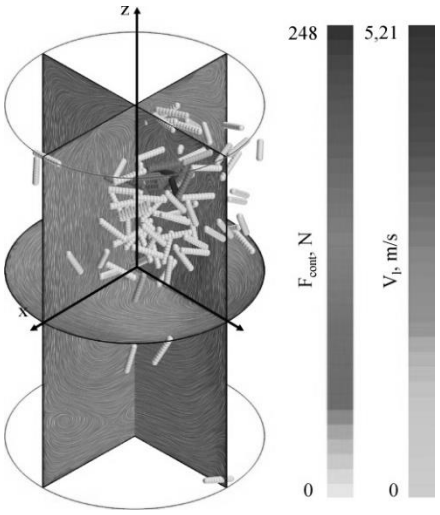

Fig. 7. Visualization of distribution of ferromagnets' contact interaction force F_{cont} under the action of rotating electromagnetic field in STAR-CCM+

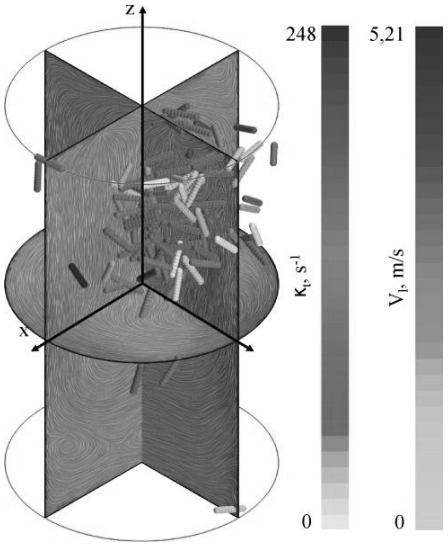

Fig. 8. Visualization of frequency of ferromagnets' impacts per time unit κ under the action of rotating electromagnetic field in STAR-CCM+

Based on the obtained data and using the Wolfram Cloud, the second-order regression equation was obtained for

– the average value of the ferromagnets' velocity V_Ω:

$$V_\Omega = 2.4802 + 0.000937\,H - 93.7\,L + 0.001848\,n + 2.676\cdot10^{-7}\,Hn - 0.02126\,N - 3.152\cdot10^{-6}\,HN - 6.172\cdot10^{-6}\,n\,N + 0.00006602\,N^2; \quad (24)$$

– the maximum force of ferromagnets' contact interaction F_{cont}:

$$F_{cont} = -659.787 + 0.0257\,H - 1,404\cdot10^{-6}\,H^2 + 27479.2\,L + 0.247917\,HL - 431852.0\,L^2 + 0.0745\,n - 9.949\cdot10^{-6}\,n^2 + 2.271\,N - 0.00378N^2; \quad (25)$$

– the frequency of ferromagnets' impacts per time unit κ:

$$\kappa = -459.9 - 0.01195\,H + 30142.1\,L + 0.561\,HL - 51092\,L^2 + 0,0392\,n + 3,44\cdot1^{-6}\,H\,n - 8.43\cdot10^{-6}\,n^2 + 0.149\,N + 0.0000453\,HN + 0.000028\,n\,N - 0.00045\,N^2. \quad (26)$$

To ensure the highest efficiency of the process of mixture components' grinding, it is required that in the vortex layer apparatus's working chamber, the ferromagnets' average velocity, their contact interaction force and the frequency of ferromagnets' impacts should be maximum:

$$\begin{cases} F_{cont}(H,n,N,L_M) \to max, \\ V_M(H,n,N,L_M) \to max, \\ \kappa(H,n,N,L_M) \to max.\{ \end{cases} \quad (27)$$

By solving compromise problem (27) together with (24), (25) and (26) in Wolfram Cloud, we obtain rational values of design-operating parameters of the vortex layer apparatus: H = 10000 A/m, n = 3825 rpm, N = 298 pcs., L_M = 0.035 mm, κ = 376 imp./s, F_{cont} = 457 N and V_M = 9.0 m/s.

Numerical modeling of the process of components' mixing in the working chamber of the vortex layer apparatus

At the third stage of theoretical research, one should investigate the process of components' mixing in the working chamber of the vortex layer apparatus. The calculation diagram with no regard to starting of rotating electromagnetic field is shown in fig. 9. In the diagram's upper part of the working chamber, two liquid flows are supplied: a mixture (by the example of pigs' liquid manure) and additional reagents. The initial velocity of the two components is different: V_{M0} for the mixture and V_{R0} for additional reagents.

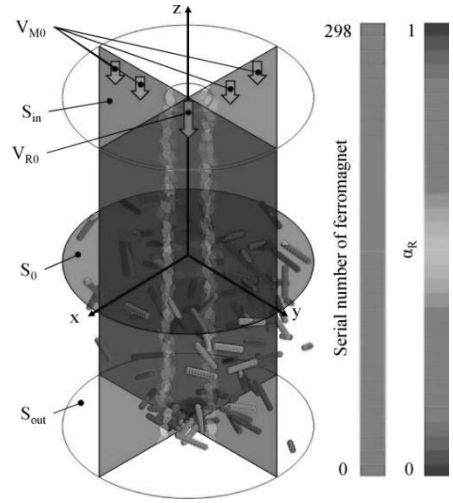

Fig. 9. Calculation diagram of component flows in the working chamber of the vortex layer apparatus with no regard to starting of rotating electromagnetic field

The components' physiomechanical properties were assumed as follows. For pigs' liquid manure: density – 1050 kg/m^3; dynamic viscosity – 0.80 Pa·s. For additional reagent: density – 1000 kg/m^3; dynamic viscosity – $8.8\cdot10^{-4}$ Pa·s. The components' interaction among themselves obeyed VOF-VOF model. For theoretical research, it was assumed that the holes for reagent supply are concentric.

In the working chamber, there are ferromagnets to the total number of N=298 pcs. The size of ferromagnets is assumed in accordance with section 2.3: L_M = 0.035 mm, D_M = 0.002 mm. The interaction between the components and ferromagnets obeyed VOF-Lagrangian phase model.

As is seen from 9–10, no mixing of component flows practically occurs.

When the rotating electromagnetic field is started, the visualization of the mixing process is obtained, which is shown in fig. 11-13.

It follows from the analysis of fig. 9–11 that, due to the ferromagnets' movement', the components' movement ' in the working chamber occurs. This causes their redistribution in the cross section, as shown in fig. 9. As the criterion for evaluation of the components' mixing process, we assume the homogeneity coefficient, which was introduced in [12]:

(28) $$\theta = 1 - \frac{1}{\alpha_{R0}} \sqrt{\frac{\sum_{i=1}^{N_\alpha} (\alpha_{Ri} - \alpha_{R0})^2}{N_\alpha - 1}}$$

where α_{Ri} is the volume fraction of additional components per volume unit on cross section S_{out}; N_α is the number of unit volumes on cross section S_{out}; α_{R0} is the required proportion of additional components per volume unit on cross section S_{out}.

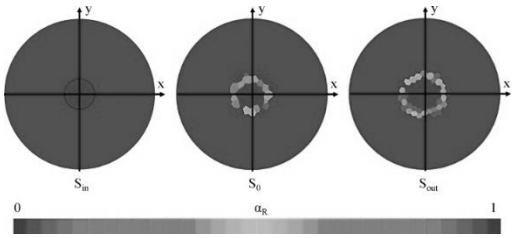

Fig. 10. Cross-sections of the working chamber of the vortex layer apparatus without regard to starting of the rotating electromagnetic field

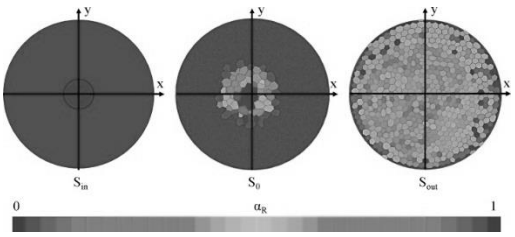

Fig. 11. Cross-sections of the working chamber of the vortex layer apparatus in the rotating electromagnetic field

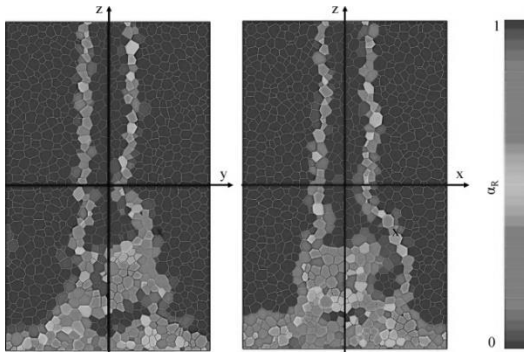

Fig. 12. Longitudinal sections of the working chamber of the vortex layer apparatus in a rotating electromagnetic field

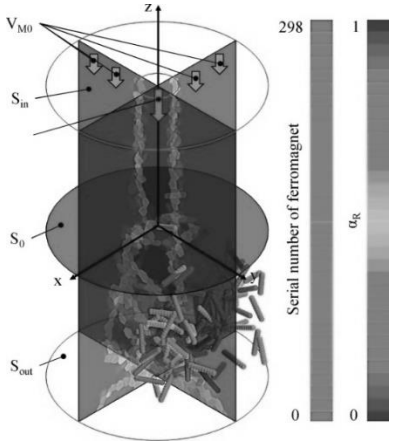

Fig. 13. Visualization of component flows in the working chamber of the vortex layer apparatus in a rotating electromagnetic field

The required proportion of additional components per volume unit is determined using the following formula:

(29) $$\alpha_{R0} = \frac{V_{R0} S_{R0}}{V_{R0} S_{R0} + V_{M0} S_{M0}}$$

where V_{R0} is the initial flow rate of liquid manure on cross section S_{in}, m/s; V_{M0} – the initial speed of the additional component supply on cross section S_{in}, m/s; S_{R0} – the area of the opening, through which liquid manure is supplied on cross section S_{in}, m^2; S_{M0} is the area of the opening, through which the additional component is supplied on cross section S_{in}, m^2.

In order to evaluate the movement of liquid and ferromagnets in the working chamber of the vortex layer apparatus in rotating electromagnetic field, respective velocity distributions were also constructed (fig. 14–15).

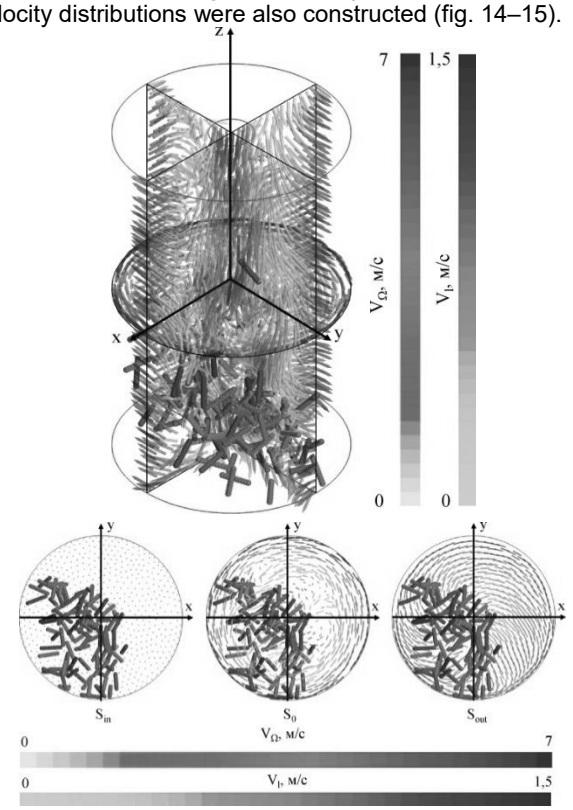

Fig. 14. Distribution of fluid and ferromagnet velocities in the working chamber of the vortex layer apparatus in rotating electromagnetic field

14–15 show the liquid's rotating movement caused by ferromagnets' movement. According to liquid's and ferromagnets' velocity distribution on cross-sections of the working chamber (fig. 12), one can assert the increase in liquid velocity on cross-section S_{out} to the value of 1.5 m/s.

The factors of numerical modeling of the process of liquid manure components' mixing in the working chamber of the vortex layer apparatus were assumed as follows: initial rates of liquid manure supply V_{R0} (1–5 m/s) and additional component V_{M0} (1–5 m/s) on cross section S_{in}.

Areas of the openings for liquid manure and additional component supply are as follows: $S_{M0} = \pi \cdot 0.005^2 = 0.0000785\ m^2$; $S_{R0} = \pi \cdot 0.045^2 - S_{M0} = 0.0055735\ m^2$.

To quantify the process under research, the volumetric productivity of mixture Q supplied through the working chamber of the vortex layer apparatus, was calculated.

As a result of numerical simulation in STAR-CCM+ according to the complete research plan ($5^2 = 25$ numerical experiments), the values of specified criteria were obtained.

Based on the data obtained and using the Wolfram Cloud, the second-order regression equation was obtained – for the mixture's homogeneity ratio θ (fig. 16):

(30) $$\theta = -1.07128 - 0.039853\ V_{M0} + 0.0035214\ V_0^2 -$$

– 0.052935 V_{R0} + 0.000925 V_{M0} V_{R0} + 0.0038 V_{R0}^2.

– the vortex layer apparatus's volumetric productivity Q (fig. 15):

(31) $Q = -2.0816 \cdot 10^{-17} + 0,0000785\ V_{M0} + 0.0062\ V_{R0}$.

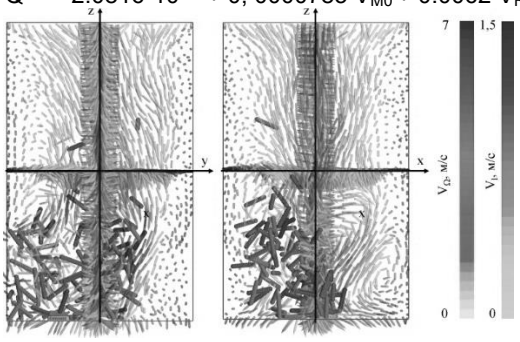

Fig. 15. Distribution of fluid velocities and ferromagnets on longitudinal sections of the working chamber of the vortex layer apparatus in rotating electromagnetic field

Dependence diagrams (30) under the condition of maximum θ (V_{R0} = 1 m/s, V_{M0} = 1 m/s) = 0.9867 are shown in Fig. 2. 28.

It follows from fig. 16 that the value of the mixture homogeneity ratio θ decreases with the increase in the components' supply velocity. This is explained by the fact that ferromagnets do not provide the mixture with required turbulence at the given parameters of rotating electromagnetic field.

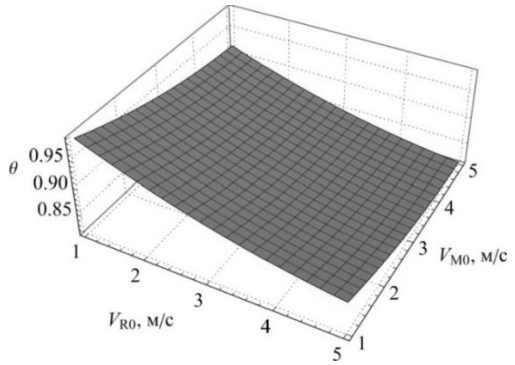

Fig. 16. Dependence between the mixture's homogeneity ratio θ and the initial rate of liquid manure supply V_{R0}, and the initial rate of additional component supply V_{M0}

Dependence diagrams (31) under the condition of maximum Q (V_{R0} = 5 m/s, V_{M0} = 5 m/s) = 0.03179 m^3/s = 114.4 m^3/h are shown in fig. 17.

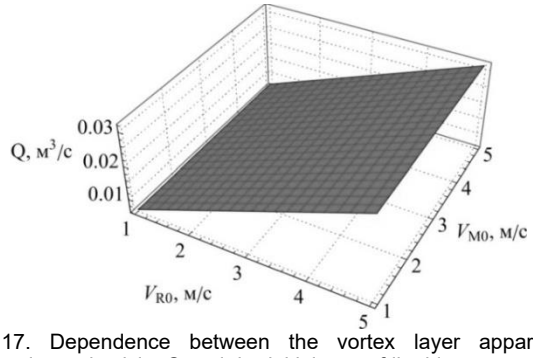

Fig. 17. Dependence between the vortex layer apparatus's volumetric productivity Q and the initial rate of liquid manure supply V_{R0} and the initial rate of the additional component supply V_{M0}

It follows from fig. 17 that with increase in the components' supply speed, the value of the volume productivity of the vortex layer apparatus Q increases, which is quite logical.

To ensure the required share of additional components α_{R0} at the maximum value of productivity of the vortex layer apparatus Q and mixture homogeneity ratio θ, one should solve the following system of equations together with (30), (31):

(32) $$\begin{cases} \alpha_{R0}(V_{R0}, V_{M0}) = \alpha_{R0}, \\ \theta(V_{R0}, V_{M0}) \to max, \\ Q(V_{R0}, V_{M0}) \to max. \end{cases}$$

By solving problem (32) in Microsoft Excel software package, we get the nomogram for calculating the components' supply velocities, which is shown in fig. 18.

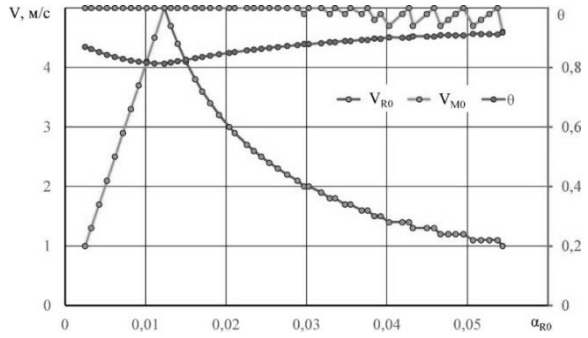

Fig. 18. Nomogram for calculating the initial rate of liquid manure supply V_{R0} and the initial rate of the additional component supply V_{M0} depending on the required share of additional components α_{R0}

In order to determine the initial rate of liquid manure supply V_{R0} and the initial rate of the additional component supply V_{M0}, one should select the value of additional components' required share α_{R0} on the abscissa axis.

Conclusions

As a result of analytical studies of rotating electromagnetic field of the vortex layer apparatus, the dependencies between the change in magnetic induction B, intensity H, as well as vector potential A of the working chamber's electromagnetic field and the coil's magnetomotive force ξ_{max}, as well as the electromagnetic field's rotation frequency n were obtained.

As a result of analytical studies of the process of interaction between cylindrical ferromagnetic elements and magnetic field in the working chamber of the vortex layer apparatus, respective physical and mathematical apparatus was modernized, which was taken as the basis for numerical modeling in Star CCM+ software package.

As a result of numerical modeling of the process of interaction between ferromagnetic elements and magnetic field in the working chamber of the vortex layer apparatus, the dependencies between changes in the average value of the ferromagnets' velocity V_{Ω}, the maximum force of their contact interaction F_{cont} and the frequency of their impacts per time unit κ and electromagnetic field strength H, its rotation frequency n, ferromagnets' number N and their length L_M were obtained. To ensure the highest efficiency of the process of liquid manure components' grinding, it is required that, in the working chamber of the vortex layer apparatus, the ferromagnets' average velocity, the strength of their contact interaction and the frequency of ferromagnets' impacts should be maximum: H = 10000 A/m, n = 3825 rpm, N = 298 pcs., L_M = 0.035 mm, κ = 376 imp./s, F_{cont} = 457 N and V_M = 9.0 m/s.

As a result of numerical modeling of the process of liquid manure components' mixing in the working chamber of the vortex layer apparatus, the dependencies between mixture

homogeneity ratio θ as well as the vortex layer apparatus's volume productivity Q and the initial rates of liquid manure V_{R0} as well as additional component V_{M0} supply were obtained. The nomogram for calculation of components' supply rates V_{R0} and V_{M0} using the value of additional components' required share α_{R0} was obtained.

Funding

This research was supported and funded by the Ministry of Education and Science of Ukraine under grant No 0121U108589.

Authors: *associate professor, candidate of technical sciences Yaropud Vitalii, Vinnytsia National Agrarian University, str. Soniachna, 3, 21008, Vinnytsia, Ukraine, E-mail: yaropud77@gmail.com; professor, doctor of technical sciences, senior researcher Aliiev Elchyn, Dnipro State Agrarian and Economic University, Serhii Efremov Str., 25, 49600, Dnipro, Ukraine, E-mail: aliev@meta.ua; graduate student Mazur Ihor, Vinnytsia National Agrarian University, str. Soniachna, 3, 21008, Vinnytsia, Ukraine, E-mail: mazurigorm77@gmail.com; PhD in engineering, senior lecturer Burlaka Serhii, Vinnytsia National Agrarian University, 21008, 3 Sonyachna str., Vinnytsia, Ukraine, e-mail: ipserhiy@gmail.com.*

REFERENCES

[1] Yaropud V.M., Hrytsun A.V., Mazur I.M. (2022). Promising technologies and technical means of processing liquid manure on pig farms. Vibrations in engineering and technology. 2022. No. 1 (104). P. 98-105.

[2] Oberemok V. M., Nikytenko M. I. (2012). Electromagnetic devices with ferromagnetic working elements. Intensification of technological processes in industrial wastewater treatment: monograph. Poltava: PUET. 318 p.

[3] Aliiev E., Pavlenko S., Golub G., Bielka O. (2022).Research of mechanized process of organic waste composting. Agraarteadus, Journal of Agricultural Science, XXXIII (1): 21–32. DOI: 10.15159/jas.22.04

[4] Aliiev E., Pavlenko S., Aliieva O., Morhun O. Accelerated biothermal composting of manure-compost mixture. Agraarteadus, Journal of Agricultural Science, 2021, XXXII (2): 169–181. DOI: 10.15159/jas.21.30

[5] Kobets A.S., Naumenko M.M., Ponomarenko N.O., Kharytonov M.M., Velychko O.P., Yaropud V.M. Design substantiation of the three-tier centrifugal type mineral fertilizers spreader. *INMATEH - Agricultural Engineering*. 2017. Vol. 53, no.3. P. 13-20.

[6] Yaropud V. (2021). Analytical Study of the Automatic Ventilation System for the Intake of Polluted Air from the Pigsty. *Scientific Horizons*. Vol. 24. No. 3. P.19-27.

[7] Paziuk V.M., Liubin M.V., Yaropud V.M., Tokarchuk O.A., Tokarchuk D.M. Research on the rational regimes of wheat seeds drying. *INMATEH - Agricultural Engineering*. 2018. Vol. 56. no.3. P. 39-48.

[8] Yaropud V., Kupchuk I., Burlaka S., Poberezhets J., Babyn I. (2022). Experimental studies of design-and-technological parameters of heat exchanger. *Przeglad Elektrotechniczny*. 2022. Vol. 98, № 10. P. 57-60.

[9] Gunko I., Babyn I., Aliiev E., Yaropud V., Hrytsun A. Research into operating modes of the air injector of the milking parlor flushing system. *U.P.B. Sci. Bull., Series D*. 2021. Vol. 83, Iss. 2, P. 297-310.

[10] Apparatus of a vortex layer with direct current electromagnets: utility model patent UA 146107: B02C 13/02, B02C 13/12, B02C 17/10. No. u 2020 05204; statement 12.08.2020; published 01/20/2021, Bulletin No. 3. 8 p.

[11] Aliev, E.B., Bandura, V.M., Pryshliak, V.M., Yaropud, V.M., Trukhanska, O.O. (2018). Modeling of mechanical and technological processes of the agricultural industry. INMATEH – Agricultural Engineering. Vol. 54, Nr. 1. P. 95-104 – ISSN 2068 – 4215.

[12] Shevchenko I. Aliiev E. (2020). Improving theefficiency ofthe process ofcontinuous flowmixing of bulkcomponents. Eastern-European Journal of Enterprise Technologies. 6/1 (108). P. 6-13. DOI: 10.15587/1729-4061.2020.216409

[13] Aliiev E., Maliehin R., Ivliev V., Aliieva O. (2021).Simulation of the process of cavitation treatment of liquid feed [Техніко-технологічне забезпечення комплексної безвідходної переробки рослинної сировини олійних культур у корми для органічного тваринництва]. Scientific Horizons, 24(2), P. 16-26. DOI: 10.48077/scihor.24(2).2021.16-26.

[14] Kupchuk I., Yaropud V., Hraniak V., Poberezhets J., Tokarchuk O., Hontar V., Didyk A. (2021).Multicriteria compromise optimization of feed grain grinding process. *Przegląd Elektrotechniczny*. Vol. 97, № 11. P. 179-183.

[15] Yaropud V., Hunko I., Aliiev E., Kupchuk I. (2021).Justification of the mechatronic system for pigsty microclimate maintenance. *Agraarteadus*. Vol. 32, № 2. P. 341-351.

[16] Rutkevych, V., Kupchuk, I., **Yaropud, V.**, Hraniak, V., Burlaka, S. Numerical simulation of the liquid distribution problem by an adaptive flow distributor. *Przeglad Elektrotechnicznythis link is disabled*. 2022. 98 (2), P. 64-69.

[17] Ibragimov R.A., Korolev E.V., Deberdeev T.R., Leksin V.V. (2019). Energy parameters of the binder during activation in the vortex layer apparatus. Materials Science Forum. 945. P. 98-103. DOI: 10.4028/www.scientific.net/MSF.945.98

[18] Honcharuk I., Kupchuk I., Yaropud V., Kravets R., Burlaka S., Hraniak V., Poberezhets Ju., Rutkevych V. (2022). Mathematical modeling and creation of algorithms for analyzing the ranges of the amplitude-frequency response of a vibrating rotary crusher in the software Mathcad. *Przeglad Elektrotechniczny*. 2022. Vol. 98 (9). P. 14-20.

[19] Bozorth R. M. (1993). Ferromagnetism. Wiley-IEEE Press. 992 p.

[20] Jamnani Dinesh. (2009). Modelling and Simulation of a Single Particle in Laminar Flow Regime of a Newtonian Liquid. Excerpt from the Proceedings of the COMSOL Conference 2009 Bangalore P. 1-9.

[21] Nail A. Gumerov, Ramani Duraiswami. (1998).Modeling of particle motion in viscous swirl flow between two porous cylinders Proceedings of FEDSM'98 1998 ASME Fluids Engineering Division Summer Meeting June 21-25,1998, Washington, DC. P. 1-8.

[22] Johnson K.L. (1987). Contact Mechanics. Cambridge University Press. 1987. 434 p.

[23] Pertti Broas. (2001). Advantages and problems of CAVE-visualisation for design purposes. Trans. VTT Symposium "Virtual prototyping". Espoo, Finland, February 1 st. pp. 73–81